EARTHQUAKE ENGINEERING AND STRUCTURAL DYNAMICS
Earthquake Engng Struct. Dyn. 2004; **33**:737–754 (DOI: 10.1002/eqe.373)

Seismic structural control using an electric servomotor active mass driver system

Chien-Liang Lee[1] and Yen-Po Wang[2,*,†]

[1]*Natural Hazard Mitigation Research Center, National Chiao-Tung University, 1001 Ta Hsueh Road, Hsinchu, Taiwan, R.O.C.*
[2]*Department of Civil Engineering, National Chiao-Tung University, 1001 Ta Hsueh Road, Hsinchu, Taiwan, R.O.C.*

SUMMARY

This study investigates an electric-type active mass driver (AMD) system for structural vibration control. Composed primarily of an electric servomotor and a ball screw, the electrical AMD system is free from noise problems, oil leakage, and labor-intensive maintenance that commonly are associated with hydraulic AMD systems. The desired stroke amplification of the mass and the power demand of the servomotor can be adjusted via the ball screw pitch, which in turn affects the effectiveness and efficiency of the system. Meanwhile, an instantaneous optimal direct output feedback control algorithm is adopted. Numerical simulation is performed using a five-story steel frame as the object structure under the conditions of the 1940 El Centro earthquake. The AMD system proves to be effective and efficient within a certain range of the ball screw pitch. The reductions of the peak responses can reach as high as 70% if properly designed. Requiring only the velocity measurement of the top floor for on-line feedback control, the proposed control algorithm is recommended for practical implementation.

KEY WORDS: active mass driver; structural control; electric servomotor; earthquake

1. INTRODUCTION

Modern earthquake protection concepts discard the traditional idea of economy-based design in favor of a performance-based design emphasizing maintenance of structural integrity, and usability of function and habitability even under exceptionally severe earthquakes. Structural control systems that have been implemented include passive, semi-active, active and hybrid devices [1–4]. Although active devices have been shown to be more robust in many aspects than passive ones, practical concerns such as the limited number of sensors and controllers,

*Correspondence to: Yen-Po Wang, Department of Civil Engineering, National Chiao-Tung University, 1001 Ta Hsueh Road, Hsinchu, Taiwan, R.O.C.
†E-mail: ypwang@mail.nctu.edu.tw

Contract grant/sponsor: National Science Council of Taiwan; contract grant/number: NSC 90-2625-Z-009-003

Received 13 April 2003
Accepted 7 October 2003

the availability of support utility systems, and the reliability of a system operating largely in a stand-by mode, still pose psychological barriers to potential users [5]. Efficiency enhancement and power savings require hardware development of the control systems, while limited sensing can be dealt with through the control algorithms.

The active devices that have been intensively studied are the active tuned mass damper (ATMD), the active mass driver (AMD) and the active bracing system (ABS) [6–8]. The active structural systems that have been practically implemented are exclusively of the ATMD or AMD types. The ATMD is a variation of the passive tuned mass damper (TMD) [9]. The TMD system is tuned in resonance with the fundamental mode of the primary structure by adjusting the stiffness of the mass damper, or the radius of the suspended pendulum, so that most of the vibrating energy is passed over to the TMD system and so dissipated. The TMD system requires a large housing space to allow for the stroking back-and-forth of the mass damper. The pendulum-type TMD is even more space-consuming when tuned for slender structures such as skyscrapers. With the auxiliary of an active control system, the ATMD system becomes more effective than its passive counterpart by robustly manipulating the damper strokes with the capability of controlling multiple vibration modes. However, the ATMD system demands actuators with a large stroking capacity, and requires a substantial power supply. Once the stroke limit of the actuator is reached during strong earthquakes, the ATMD system could be locked up for self-protection, which as a result can cause a malfunction of the control systems, as observed during the 1995 Kobe earthquake, Japan. The AMD system, on the other hand, is similar to the ATMD, except that it requires no tuning with the primary structure. As the AMD system is not responding resonantly to the primary structure, the stroke demand on the actuator is considerably reduced in comparison with the ATMD.

An AMD system normally comprises of an actuator (either hydraulic or electric type), a servo-control system, a mass block, vibration sensors and a data acquisition system. Despite the fact that hydraulic-type AMD systems have been studied extensively in the laboratory [10–12], they are not favorable from a practical point of view due to problems of noise, oil leakage, and high maintenance requirements. Moreover, the peripheral equipment such as the hydraulic pump, accumulator and pipelines require additional space. On the other hand, electric servomotors are relatively clean and easy to maintain. With the rapid and revolutionary progress in power electronics and microelectronics, the commercially available AC or DC servomotors nowadays have sufficient capacity for industrial applications.

Servomotors [13–16] transform electric power into mechanical dynamics. The servomotors can be categorized into direct current (DC) motors and alternating current (AC) motors. The permanent magnet brush DC servomotor is composed of a rotor wound with coils, a stator of ferrite permanent magnet in the external frame and a mechanical commutator with switch brushes. Torque is generated via the interaction between the current and the magnetic field, as the current in the electric conductor flows through the brushes of the commutator to the coils in the magnetic field. Commutation sparks, however, may arise from the friction between the commutator and brushes, and therefore the brushes require frequent maintenance. The brushless AC servomotor uses external semiconductor switching circuits (transistors and thyristors) instead of a mechanical commutator to generate alternating currents. For the AC servomotor, the rotor is made of a permanent magnet, and the stator is a wound coil of single or three phases. A highly efficient AC servomotor that supplies torque rather smoothly is devised by

using a three-phase coil, which at each phase transforms the current into sine waves. These three-phase alternating sine wave currents flowing in the coils are adjusted in accordance with the rotor position detected by the encoders or resolvers. Modern servomotors are implanted with digital signal processors for motion control to meet the increasingly stringent performance criteria. Servomotors are now lightweight, compact, easily integrated, efficient, controllable, less noisy, and nearly maintenance-free. In Japan, active mass dampers driven by AC servomotors have been implemented in several tall buildings for vibration control against high winds or earthquakes [17–20].

The AMD system investigated in this study is composed primarily of an AC servomotor and a ball screw. The ball screw, connected with a coupling in series, is used as the transmission media to convert the rotational motion of the motor into translation movement [21, 22]. As the servomotor rotates one revolution counterclockwise, the mass block is advanced one pitch of the ball screw. The pitch distance of the ball screw is therefore proportional to the AMD stroke, which in turn affects the control performance of the AMD system.

In this paper, the effect of the pitch distance of the ball screw on the performance of the electrical AMD system is explored. Meanwhile, an instantaneous optimal direct output feedback control algorithm [23] is adopted. Numerical simulation is carried out using a five-story steel frame as the object structure under the conditions of the 1940 El Centro earthquake. The AMD system proves to be effective and efficient within a certain range of the ball screw pitch. The reductions of the peak responses can reach as high as 70% if properly designed. Requiring only the velocity measurement of the top floor for on-line feedback control, the proposed control algorithm is recommended for practical implementation.

2. MECHANISM OF THE ACTIVE MASS DRIVER SYSTEM

The AMD system investigated in this study is composed primarily of an AC servomotor, a ball screw and a mass block, as shown in Figure 1. The ball screw (Figure 2) connected in series with a coupling (Figure 3) is used as the transmission medium to convert the rotational motion of the motor into translational movement. As the servomotor rotates one revolution counterclockwise, the mass block is advanced one pitch of the ball screw. The friction between the interfaces of the screw and its supports can be minimized with the bearing balls circulating in the hardened steel races, formed by concave helical grooves and the mating nut. As the screw and nut rotate against each other, the bearing balls are diverted from one end to the opposite end of the ball nut via the guiding return tubes. This re-circulation process permits an unrestricted traveling of the nut around the screw. The mass block, carried by four roller bearings, is connected with the nut on the ball screw, which drives it on the rail in a linear motion. The pitch distance of the ball screw is proportional to the AMD stroke. The maximum stroke of the mass block is ± 10 cm constrained by the unseating-prevention switches. The servomotor is designed to stop without shutting down the power as the mass block hits the unseating-prevention switches, until the mass block reverses its direction.

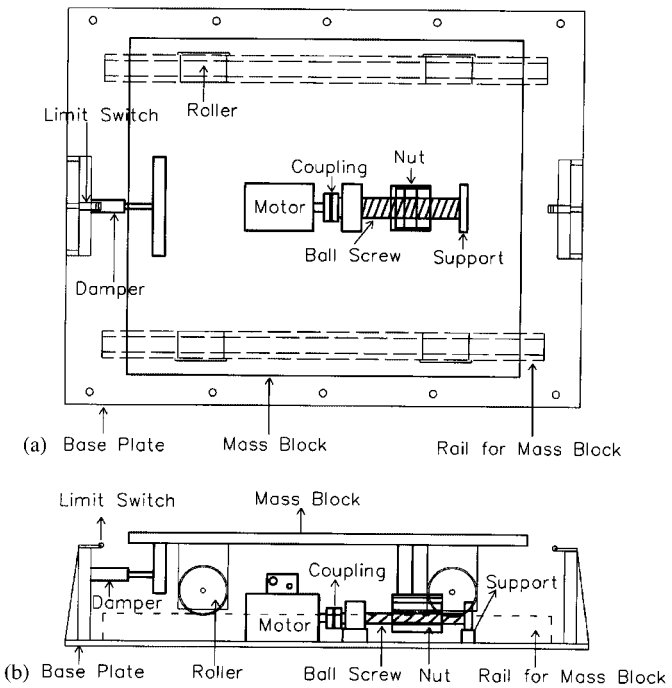

Figure 1. Configuration of the AMD System: (a) top view; and (b) side view.

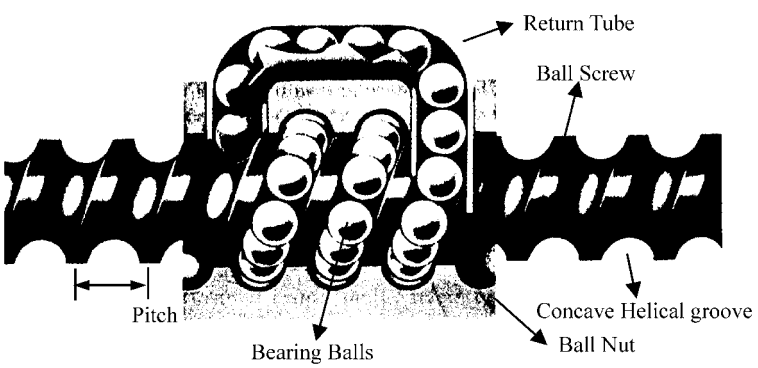

Figure 2. Components of ball screw [22].

3. DYNAMICS OF THE AMD SYSTEM

A structural dynamic system implemented with an active mass driver system and subjected to external disturbance, $\mathbf{w}(t)$, and control force, $u(t)$, can be described as:

$$\mathbf{M}\ddot{\mathbf{x}}(t) + \mathbf{C}\dot{\mathbf{x}}(t) + \mathbf{K}\mathbf{x}(t) = -\mathbf{E}\mathbf{w}(t) + \mathbf{B}u(t) \tag{1}$$

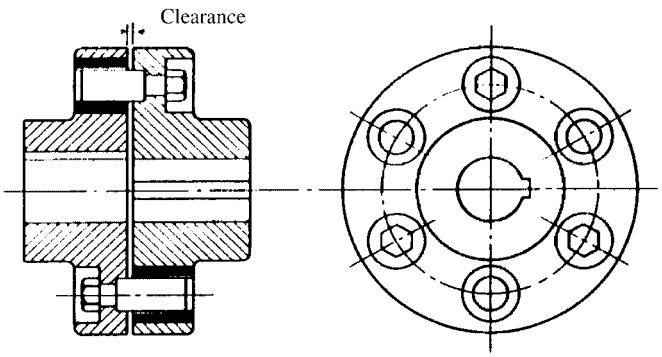

Figure 3. Coupling [22].

where $\mathbf{x}$ is the $n \times 1$ displacement vector, $\mathbf{M}$ is the $n \times n$ mass matrix, $\mathbf{C}$ is the $n \times n$ damping matrix, $\mathbf{K}$ is the $n \times n$ stiffness matrix, $\mathbf{w}(t)$ is the $q \times 1$ disturbance vector, E is the $n \times q$ location matrix of the external disturbances, $u(t)$ is the control force and $\mathbf{B}$ is the $n \times 1$ location matrix of the control forces.

The control force, $u(t)$, can be further expressed in terms of the torque, $u_T(t)$, of the servomotor. As the servomotor rotates one revolution, the mass block is advanced one pitch of the ball screw. Hence, the stroke of the mass block relative to the attached floor can be calculated as:

$$\bar{x}_a = x_a - x_n = \mathbf{L}^T \mathbf{x} = \frac{l_b \theta_m}{2\pi} \tag{2}$$

where $\bar{x}_a$ is the stroke of the mass block relative to the roof; x_a is the displacement of the mass block relative to the ground; x_n is the roof displacement of the structure relative to the ground; $\mathbf{L} = [1 \quad -1 \quad \mathbf{0}_{1\times(n-2)}]^T$ is the $n \times 1$ location vector; θ_m is the angular rotation of the servomotor; and l_b is the pitch distance of the ball screw. The velocity of the mass block relative to the roof can be calculated by taking the derivatives of both sides of Equation (2) with respect to time t as:

$$\dot{\bar{x}}_a = \mathbf{L}^T \dot{\mathbf{x}} = \frac{l_b}{2\pi} \dot{\theta}_m = \frac{l_b}{2\pi} \omega_m \tag{3}$$

where $\dot{\bar{x}}_a$ is the velocity of the mass block relative to the roof; and $\omega_m = \dot{\theta}_m$ (rad/sec) is the angular velocity of the servomotor. Similarly, the acceleration of the mass block relative to the roof can be represented as:

$$\ddot{\bar{x}}_a = \mathbf{L}^T \ddot{\mathbf{x}} = \frac{l_b}{2\pi} \dot{\omega}_m = \frac{l_b}{2\pi} \alpha_m \tag{4}$$

where $\ddot{\bar{x}}_a$ is the acceleration of the mass block relative to the roof, and $\dot{\omega}_m = \ddot{\theta}_m = \alpha_m$ (rad/sec)^2 is the angular acceleration of the servomotor. Assuming conservation of energy, the work done by the servomotor in one revolution is equal to that of the mass block advancing one pitch. Therefore, the torque, u_T, supplied by the servomotor and the translation force, u, applied to

the mass block satisfies

$$u_{\mathrm{T}} = \frac{l_{\mathrm{b}}}{2\pi} u \tag{5}$$

The reaction force of u to the structure is the active control force. If the inertia of the rotating components, including the rotor of the servomotor, the ball screw and the coupling are taken into account, equilibrium of the torque is modified as:

$$\begin{aligned} u_{\mathrm{T}} &= \frac{l_{\mathrm{b}}}{2\pi} u + (J_{\mathrm{M}} + J_{\mathrm{B}} + J_{\mathrm{C}})\alpha_{\mathrm{m}} \\ &= \frac{l_{\mathrm{b}}}{2\pi} u + \bar{J}\alpha_{\mathrm{m}} \end{aligned} \tag{6}$$

where J_{M}, J_{B} and J_{C} are, respectively, the mass moments of inertia of the rotor of the servomotor, the ball screw and the coupling; $\bar{J} = J_{\mathrm{M}} + J_{\mathrm{B}} + J_{\mathrm{C}}$ is the sum of the mass moments of inertia of the rotating parts. Substituting Equation (4) into Equation (6), the torque supplied by the servomotor can be expressed as:

$$u_{\mathrm{T}} = \frac{l_{\mathrm{b}}}{2\pi} u + \frac{2\pi}{l_{\mathrm{b}}} \bar{J}\mathbf{L}^{\mathrm{T}}\ddot{\mathbf{x}} \tag{7}$$

Moreover, the active control force applied to the structure can be calculated from Equation (7) as:

$$u = \frac{2\pi}{l_{\mathrm{b}}} u_{\mathrm{T}} - \left(\frac{2\pi}{l_{\mathrm{b}}}\right)^2 \bar{J}\mathbf{L}^{\mathrm{T}}\ddot{\mathbf{x}} \tag{8}$$

By substituting the active control force from Equation (8) into Equation (1), the equation of motion of the dynamic system implemented with the AMD system driven by the servomotor, can be expressed as:

$$\bar{\mathbf{M}}\ddot{\mathbf{x}}(t) + \mathbf{C}\dot{\mathbf{x}}(t) + \mathbf{K}\mathbf{x}(t) = -\mathbf{E}\mathbf{w}(t) + \bar{\mathbf{B}}u_{\mathrm{T}}(t) \tag{9}$$

where $\bar{\mathbf{M}} = \mathbf{M} + (2\pi/l_{\mathrm{b}})^2 \bar{J}\mathbf{B}\mathbf{L}^{\mathrm{T}}$ is the $n \times n$ modified mass matrix, taking into account the inertia of the rotating parts of the AMD system; and $\bar{\mathbf{B}} = (2\pi/l_{\mathrm{b}})\mathbf{B}$ is the $n \times 1$ location matrix of the control torques supplied by the servomotor. The optimal design of the pitch distance will be determined through the parametric studies to be discussed later in this paper.

4. INSTANTANEOUS OPTIMAL DIRECT OUTPUT FEEDBACK CONTROL

4.1. Discrete-time state-space system

Equation (9) can be further represented in a state-space form, leading to a first-order differential equation as:

$$\dot{\mathbf{z}}(t) = \mathbf{A}_{\mathrm{c}}\mathbf{z}(t) + \mathbf{B}_{\mathrm{c}}u_{\mathrm{T}}(t) + \mathbf{E}_{\mathrm{c}}\mathbf{w}(t) \tag{10}$$

where $\mathbf{Z}(t) = \begin{bmatrix} \mathbf{x}(t) \\ \dot{\mathbf{x}}(t) \end{bmatrix}$ is the $2n \times 1$ state vector, $\mathbf{A}_c = \begin{bmatrix} \mathbf{0} & \mathbf{I} \\ -\tilde{\mathbf{M}}^{-1}\mathbf{K} & -\tilde{\mathbf{M}}^{-1}\mathbf{C} \end{bmatrix}$ is the $2n \times 2n$ continuous-time system matrix, $\mathbf{E}_c = \begin{bmatrix} \mathbf{0} \\ \tilde{\mathbf{M}}^{-1}\mathbf{E} \end{bmatrix}$ is the $2n \times q$ continuous-time location matrix of the external disturbances, and $\mathbf{B}_c = \begin{bmatrix} \mathbf{0} \\ \tilde{\mathbf{M}}^{-1}\tilde{\mathbf{B}} \end{bmatrix}$ is the $2n \times 1$ continuous-time location matrix of the control forces.

If a first-order interpolation of the functions, $u_T(\tau)$ and $\mathbf{w}(\tau)$, within any two consecutive sampling points $[k-1, k]$ is considered, then Equation (10) can further be resolved into a recursive discrete-time state equation as:

$$\mathbf{Z}[k] = \mathbf{A}\mathbf{Z}[k-1] + (\mathbf{P}_1 + \mathbf{P}_2)(\mathbf{B}_c u_T[k] + \mathbf{E}_c \mathbf{w}[k]) - \mathbf{P}_2(\mathbf{B}_c u_T[k-1] + \mathbf{E}_c \mathbf{w}[k-1]) \tag{11}$$

where

$$\mathbf{A} = \mathbf{I} + \mathbf{A}_c \varphi \Delta t \tag{12}$$

$$\mathbf{P}_1 = \varphi \Delta t \tag{13}$$

$$\mathbf{P}_2 = \Phi - \varphi \Delta t \tag{14}$$

$$\varphi = \mathbf{I} + \mathbf{A}_c \tag{15}$$

$$\Phi = \frac{\Delta t}{2}\left[\mathbf{I} + \mathbf{A}_c \frac{\Delta t}{3}\left[\cdots \mathbf{A}_c \frac{\Delta t}{n-1}\left[\mathbf{I} + \mathbf{A}_c \frac{\Delta t}{n}\right]\right]\cdots\right] \tag{16}$$

and $\mathbf{I}$ is a unit matrix. Since Equation (16) is represented in a nested form, the derivation of the discrete-time system matrix, $\mathbf{A}$ and the rest requires no inverse of the continuous-time system matrix $\mathbf{A}_c^{-1}$. Therefore, they can be obtained even if matrix $\mathbf{A}_c$ is singular, as is the case of the AMD-controlled structure where the AMD system contributes no stiffness.

4.2. Direct output feedback control algorithm

Since the transient disturbance function, $\mathbf{w}[k]$ in the discrete-time state equation (11) cannot be predicted in advance during an earthquake episode, this term is therefore neglected in the control design of the active system, and the state equation (11) is reduced as:

$$\mathbf{Z}[k] = \mathbf{B}_1 u_T[k] + \mathbf{s}[k-1] \tag{17}$$

where

$$\mathbf{s}[k-1] = \mathbf{A}\mathbf{Z}[k-1] - \mathbf{P}_2 \mathbf{B}_c u_T[k-1] \tag{18}$$

and

$$\mathbf{B}_1 = (\mathbf{P}_1 + \mathbf{P}_2)\mathbf{B}_c \tag{19}$$

Now, if determination of the optimal feedback control forces is based only on partial output state, $\mathbf{y}[k]$, as:

$$u_T[k] = \mathbf{G}\mathbf{y}[k] = \mathbf{G}\mathbf{D}\mathbf{Z}[k] \tag{20}$$

where $\mathbf{y}[k]$ is the $r \times 1$ output state vector ($r \leqslant 2n$), and $\mathbf{D}$ is the $2n \times r$ location matrix of the output state, then it can lead from Equations (17), (18) and (20) to

$$\mathbf{Z}[k] = (\mathbf{I} - \mathbf{B}_1\mathbf{G}\mathbf{D})^{-1}\mathbf{s}[k-1] \tag{21}$$

Define the instantaneous performance index, $J[k]$, for any time instant k as

$$J[k] = \mathbf{Z}^{\mathrm{T}}[k]\mathbf{Q}\mathbf{Z}[k] + u_{\mathrm{T}}^{\mathrm{T}}[k]\mathbf{R}u_{\mathrm{T}}[k] \tag{22}$$

where the weighting matrices $\mathbf{Q}$ and $\mathbf{R}$ are semi-positive definite and positive definite, respectively, so that an optimal solution exists. In this paper, the weighting matrix $\mathbf{Q} = \begin{bmatrix} \mathbf{K} & \mathbf{0} \\ \mathbf{0} & \mathbf{M} \end{bmatrix}$ is adopted to reserve meaningful physical interpretations of the first term on the R.H.S. of Equation (22), as the sum of strain energy and kinetic energy of the vibrating structure. $\mathbf{R}$ reduces to a scalar, since only a single AMD system is implemented.

Substitution of Equations (20) and (21) into Equation (22) leads to:

$$J[k] = \mathbf{s}^{\mathrm{T}}[k-1]\mathbf{H}\mathbf{s}[k-1] \tag{23}$$

where

$$\mathbf{H} = (\mathbf{I} - \mathbf{B}_1\mathbf{G}\mathbf{D})^{-\mathrm{T}}(\mathbf{Q} + \mathbf{D}^{\mathrm{T}}\mathbf{G}^{\mathrm{T}}\mathbf{R}\mathbf{G}\mathbf{D})(\mathbf{I} - \mathbf{B}_1\mathbf{G}\mathbf{D})^{-1} \tag{24}$$

It is noted that $J[k] \geqslant 0$, since energy is non-negative. If $\eta_1, \eta_2, \eta_3, \ldots, \eta_{2n}$ are the eigenvalues of matrix $\mathbf{H}$, then J is minimum as $\eta_1 + \eta_2 + \eta_3 + \ldots \eta_{2n}$ is minimum, for $J[k] \geqslant 0$. That is,

$$\frac{\mathrm{d}J}{\mathrm{d}\mathbf{G}} = \frac{\mathrm{d}(\eta_1 + \eta_2 + \eta_3 + \cdots + \eta_{2n})}{\mathrm{d}\mathbf{G}} = \frac{\mathrm{d}\,tr(\mathbf{H})}{\mathrm{d}\mathbf{G}} = \mathbf{0}_{1\times 2n} \tag{25}$$

The feedback gain matrix, $\mathbf{G}$, can hence be resolved from Equation (25) as:

$$\begin{aligned}\mathbf{G} = &-\mathbf{R}^{-1}\mathbf{B}_1^{\mathrm{T}}(\mathbf{I} - \mathbf{B}_1\mathbf{G}\mathbf{D})^{-\mathrm{T}}(\mathbf{Q} + \mathbf{D}^{\mathrm{T}}\mathbf{G}^{\mathrm{T}}\mathbf{R}\mathbf{G}\mathbf{D})(\mathbf{I} - \mathbf{B}_1\mathbf{G}\mathbf{D})^{-1}(\mathbf{I} - \mathbf{B}_1\mathbf{G}\mathbf{D})^{-\mathrm{T}}\mathbf{D}^{\mathrm{T}} \\ &\times[\mathbf{D}(\mathbf{I} - \mathbf{B}_1\mathbf{G}\mathbf{D})^{-1}(\mathbf{I} - \mathbf{B}_1\mathbf{G}\mathbf{D})^{-\mathrm{T}}\mathbf{D}^{\mathrm{T}}]^{-1}\end{aligned} \tag{26}$$

4.3. Numerical solution for the feedback gain matrix [*23*]

The gain matrix $\mathbf{G}$ in Equation (26) is not expressed explicitly; therefore, it can only be obtained numerically based on an iterative procedure as follows:

(1) $i = 1$
(2) Let $\mathbf{G}^{(i)} = \mathbf{0}$
(3) $\tilde{\mathbf{G}}^{(i)} = -\mathbf{R}^{-1}\mathbf{B}_1^{\mathrm{T}}(\mathbf{I} - \mathbf{B}_1\mathbf{G}^{(i)}\mathbf{D})^{-\mathrm{T}}(\mathbf{Q} + \mathbf{D}^{\mathrm{T}}\mathbf{G}^{(i)^{\mathrm{T}}}\mathbf{R}\mathbf{G}^{(i)}\mathbf{D})(\mathbf{I} - \mathbf{B}_1\mathbf{G}^{(i)}\mathbf{D})^{-1}(\mathbf{I} - \mathbf{B}_1\mathbf{G}^{(i)}\mathbf{D})^{-\mathrm{T}}\mathbf{D}^{\mathrm{T}}$
$[\mathbf{D}(\mathbf{I} - \mathbf{B}_1\mathbf{G}^{(i)}\mathbf{D})^{-1}(\mathbf{I} - \mathbf{B}_1\mathbf{G}^{(i)}\mathbf{D})^{-\mathrm{T}}\mathbf{D}^{\mathrm{T}}]^{-1}$
(4) $\tilde{\mathbf{G}}^{(i+1)} = \frac{\mathbf{G}^{(i)} + \lambda\tilde{\mathbf{G}}^{(i)}}{1+\lambda}$ (λ is a progressive step factor. The smaller the factor, the slower the rate of convergence, but with a better stability).
(5) Stop iteration if $|\mathbf{G}^{(i+1)} - \mathbf{G}^{(i)}| \leqslant \varepsilon$ where ε is the tolerance of error.
(6) $i = i + 1$, go to step (3).

5. NUMERICAL EXAMPLE

5.1. System modeling

The objective structure considered for assessment of the AMD system is a half-scaled 5-story steel frame model. System parameters of the model structure are summarized in Table I.

Considering that the electrical AMD system is placed on the roof of the model structure for seismic response control, the parameters in system equation (9) can further be expressed as:

$\mathbf{x} = \begin{bmatrix} x_a \\ \mathbf{x}_s \end{bmatrix}$ is the 6×1 displacement vector, where x_a is the displacement of the mass block (relative to the ground), and $\mathbf{x}_s$ is the displacement vector of the structure (relative to the ground);

$\bar{\mathbf{M}} = \begin{bmatrix} m_a & \mathbf{0} \\ \mathbf{0} & \mathbf{M}_s \end{bmatrix} + \left(\frac{2\pi}{l_b}\right)^2 \bar{J}\mathbf{B}\mathbf{L}^T$ is the 6×6 mass matrix, where $\mathbf{M}_s$ is the mass matrix of the structure, and $m_a = 400\,\text{kg}$ is the mass of the mass block, which is about 10% of the structure's total mass; $\bar{J} = 0.0018\,\text{kg} \cdot \text{s}^2 \cdot \text{m}$ is the rotational inertia of the servomotor system; $\mathbf{L} = -\mathbf{B} = [1 \quad -1 \quad 0 \quad 0 \quad 0 \quad 0]^T$;

$\mathbf{C} = \begin{bmatrix} c_a & -c_a\bar{\mathbf{L}}^T \\ -c_a\bar{\mathbf{L}} & \mathbf{C}_s + \bar{\mathbf{L}}c_a\bar{\mathbf{L}}^T \end{bmatrix}$ is the 6×6 damping matrix, where $\mathbf{C}_s$ is the damping matrix of the structure, $c_a = 204.96\,\text{kg} \cdot \text{s/m}$ is the damping coefficient of the AMD system, and $\bar{\mathbf{L}} = [1 \quad 0 \quad 0 \quad 0 \quad 0]^T$;

Table I. System parameters of the 5-story model structure.

Mode	1	2	3	4	5
Frequency (Hz)	2.79	9.58	17.83	27.22	36.09
Damping ratio (%)	0.35	3.44	2.63	2.91	3.21
Mode shapes					
5f	0.5667	−0.4994	0.4455	−0.0868	−0.4943
4f	0.6314	−0.1747	−0.1903	0.0275	0.7257
3f	0.3580	0.2274	−0.7430	−0.2589	−0.4423
2f	0.3247	0.7856	0.4600	−0.2422	0.0356
1f	0.2159	0.2266	−0.0408	0.9306	−0.1794
System matrices					
Mass matrix	82.03	0	0	0	0
($\text{kg} \cdot \text{s}^2/\text{m}$)	0	84.32	0	0	0
	0	0	84.32	0	0
	0	0	0	84.32	0
	0	0	0	0	84.68
Stiffness matrix	1307200	−1581400	610500	75100	134400
(kg/m)	−1581400	2358800	−1274200	−33600	−507600
	610500	−1274200	1625200	−220500	−196500
	75100	−33600	−220500	567300	−547300
	134400	−507600	−196500	−547300	2306500
Damping matrix	471.65	−440.90	83.43	−36.69	−5.44
($\text{kg} \cdot \text{s/m}$)	−440.90	684.32	−343.50	−63.44	−148.62
	83.43	−343.50	593.06	−73.81	−69.73
	−36.69	−63.44	−73.81	374.31	−143.03
	−5.44	−148.62	−69.73	−143.03	790.01

$\mathbf{K} = \begin{bmatrix} k_a & -k_a\bar{\mathbf{L}}^T \\ -k_a\bar{\mathbf{L}} & \mathbf{K}_s + \bar{\mathbf{L}}k_a\bar{\mathbf{L}}^T \end{bmatrix}$ is the 6×6 stiffness matrix, where $\mathbf{K}_s$ is the stiffness matrix of the structure, and k_a is the stiffness of the AMD system $k_a = 0$ in the present case);

$\mathbf{E} = \begin{bmatrix} m_a \\ \mathbf{m}_s 1 \end{bmatrix}$ is the 6×1 location matrix of the earthquake force with $\mathbf{1} = [1\ 1\ 1\ 1\ 1]^T$; and

$\bar{\mathbf{B}} = \frac{2\pi}{l_b}\mathbf{B}$ is the 6×1 location matrix of the control force in terms of torque.

Substituting Equation (21) for $\mathbf{Z}[k]$ into Equation (11), the discrete-time state-space equation can further be written as:

$$\mathbf{Z}[k] = \mathbf{A}_u\mathbf{Z}[k-1] + \mathbf{E}_1\mathbf{w}[k] + \mathbf{E}_o\mathbf{w}[k-1] \tag{27}$$

in which

$$\mathbf{A}_u = (\mathbf{I} - \mathbf{B}_1\mathbf{G}\mathbf{D})^{-1}(\mathbf{A} - \mathbf{P}_2\mathbf{B}_c\mathbf{G}\mathbf{D}) \tag{28}$$

$$\mathbf{E}_1 = (\mathbf{I} - \mathbf{B}_1\mathbf{G}\mathbf{D})^{-1}(\mathbf{P}_1 + \mathbf{P}_2)\mathbf{E}_c \tag{29}$$

$$\mathbf{E}_0 = -(\mathbf{I} - \mathbf{B}_1\mathbf{G}\mathbf{D})^{-1}\mathbf{P}_2\mathbf{E}_c \tag{30}$$

Equation (27) serves as the basis for assessing the performance of the active structural control system. Through eigenvalue analysis of the effective system matrix, $\mathbf{A}_u$, the equivalent modal frequencies and damping factors of the system can be evaluated. Whether or not the control design is sufficient can be ascertained by the dynamic characteristics extracted from $\mathbf{A}_u$.

In this study, only the top floor velocity ($\dot{x}_5$) is considered as the output feedback state in determining the optimal control force. The 1940 El Centro earthquake (N–S) is used as the input disturbance.

5.2. Performance assessment in the frequency-domain analysis

The dynamic characteristics of the structure implemented with the AMD system are first examined via eigenvalue analysis for $l_b = 1, 2, 4, 8, 10$cm and $R = 10^{-2.4}$. As Table II shows, the equivalent damping ratios of the structure implemented with the AMD system are significantly enhanced, especially for the first three modes. The optimum case appears as $l_b = 4$ cm, where the equivalent modal damping ratio of the first mode is greatly enhanced from 0.35% to 71.84%, from 3.44% to 15.78% for the second mode, and from 2.63% to 7.73% for the third mode. Moreover, it is observed that the frequencies of the model structure are only slightly changed as the AMD is implemented. The AMD system improves the dynamic characteristics of the structure by significantly increasing its damping capabilities while maintaining the original stiffness. Despite the fact that only the velocity of the roof is measured as the feedback state, no spillover is observed when using the proposed direct output feedback control law.

The effectiveness of the AMD with various pitch sizes is also revealed from the frequency response functions of the roof acceleration (Figure 4(a)) and the roof displacement (Figure 4(b)) in which the peaks of the transfer function are greatly suppressed. The control efficiency is evidently varied with the pitch. The optimum case again occurs at $l_b = 4$ which is consistent with that from the eigenvalue analysis.

Table II. Summary of eigenvalue analysis ($m_a = 400\,\text{kg}$, $R = 10^{-2.4}$).

Mode	Without control	$l_b = 1$ cm	$l_b = 2$ cm	$l_b = 4$ cm	$l_b = 8$ cm	$l_b = 10$ cm
			Frequency (Hz)			
1	2.79	2.60	2.62	2.56	2.42	2.50
2	9.58	9.12	9.09	8.94	9.20	9.32
3	17.83	17.24	17.29	17.31	17.56	17.66
4	27.22	27.18	27.19	27.20	27.22	27.22
5	36.09	34.84	35.23	36.03	36.53	36.51
			Damping (%)			
1	0.35	10.59	33.31	71.84	56.48	41.84
2	3.44	5.21	9.55	15.78	14.28	12.16
3	2.63	3.29	5.00	7.73	7.50	6.65
4	2.91	2.93	2.97	3.05	3.04	3.02
5	3.21	3.46	4.40	6.30	6.27	5.69

5.3. *Performance assessment in the time domain*

In this section, the effects of the pitch size of the ball screw on the performance of the system are further explored. Control efficiency at various pitch distances (l_b) of the ball screw for various weighting factors (R) is first assessed. Figure 5 illustrates the efficiency curves in terms of peak reduction of roof acceleration. The control efficiency increases as R decreases, while the optimum cases occur as the pitch of the ball screw $l_b = 4\,\text{cm}$, regardless of R. For the case of $R = 10^{-2.4}$ with $l_b = 4\,\text{cm}$, a reduction of 71% has been achieved. The efficiency curves in terms of peak reduction of roof displacement and structural response index (SRI) are shown in Figures 6 and 7, respectively. The SRI is defined as the sum of the strain energy and the kinetic energy of the structure at each time instant over the entire response history. Again, the control efficiency increases as R decreases. The trend of variation of the curves is similar to those for the roof acceleration, except that the optimum cases occur at $l_b = 5\,\text{cm}$, regardless of R. For the case of $R = 10^{-2.4}$ with $l_b = 5\,\text{cm}$, a peak reduction of roof displacement by 76% and SRI by 88% has been achieved.

The maximum AMD stroke at various pitch distances (l_b) for various weighting factors (R) is illustrated in Figure 8. Similar to the control efficiency curves, the AMD stroke increases as R decreases. This indicates that the more robust the AMD is activated, the better the control performance is achieved. The maximum AMD stroke occurs at $l_b = 5\,\text{cm}$, regardless of R. For the case of $R = 10^{-2.4}$ with $l_b = 5\,\text{cm}$, the maximum stroke of the AMD system is $\bar{x}_a = 8.81\,\text{cm}$.

The maximum torque, the maximum control force and the maximum power demand of the AMD system at various pitch distances (l_b) for various weighting factors (R) are also evaluated. The maximum torque shown in Figure 9, similar to the control efficiency curves, increases as R decreases. For the case of $R = 10^{-2.4}$ with $l_b = 4\,\text{cm}$ or $l_b = 5\,\text{cm}$, where the optimum control efficiencies occur, the maximum torque demanded from the servomotor is minimal. This indicates that the AMD system is not only effective but also efficient when the pitch size of the ball screw is adjusted appropriately. The maximum control force presented in Figure 10 increases as R decreases, while it tends to decrease with the pitch size, regardless of R. The maximum control force is evidently varied with the pitch. Owing to the fact that

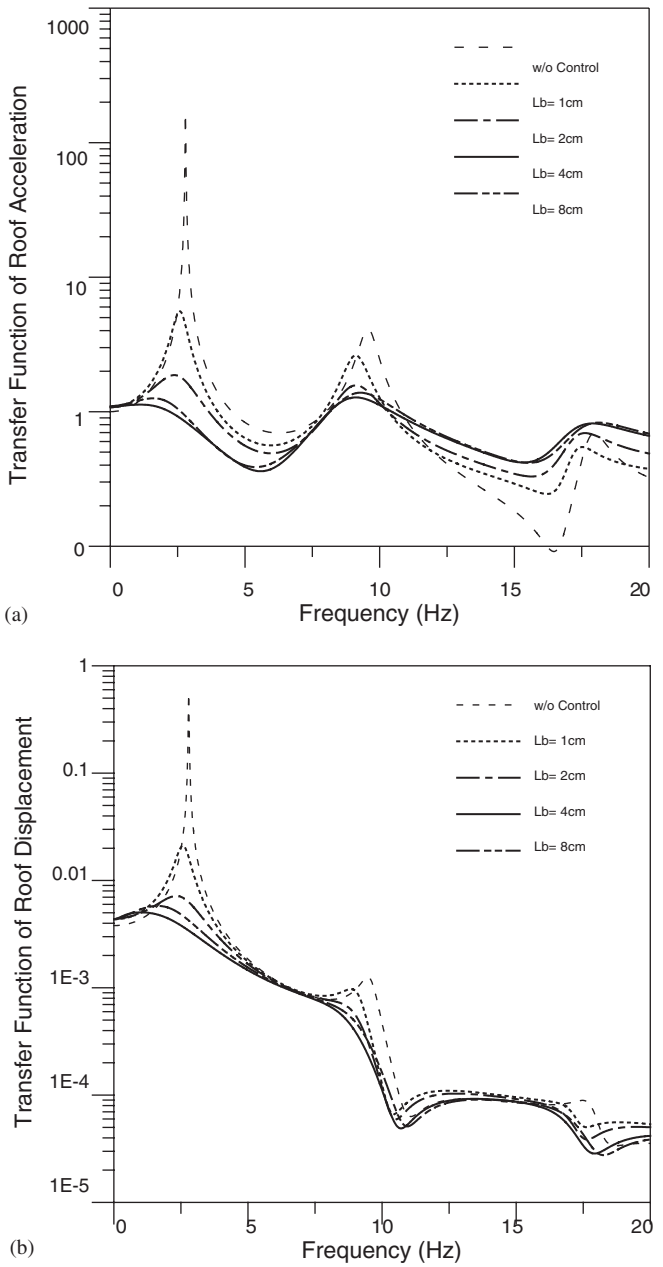

Figure 4. (a) Comparison of roof acceleration frequency responses ($R = 10^{-2.4}$); and (b) comparison of roof displacement frequency responses ($R = 10^{-2.4}$).

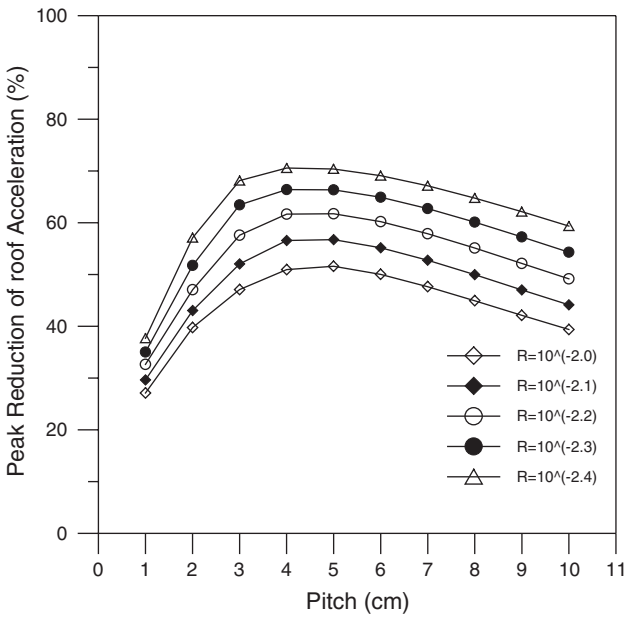

Figure 5. Efficiency curves of roof acceleration response.

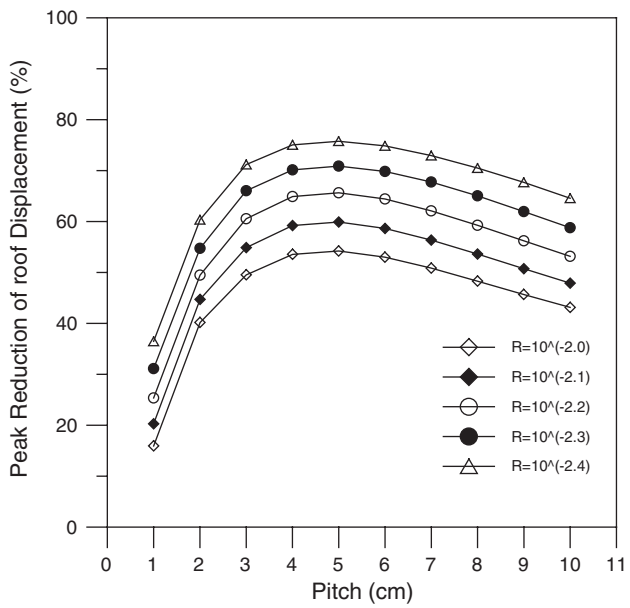

Figure 6. Efficiency curves of roof displacement response.

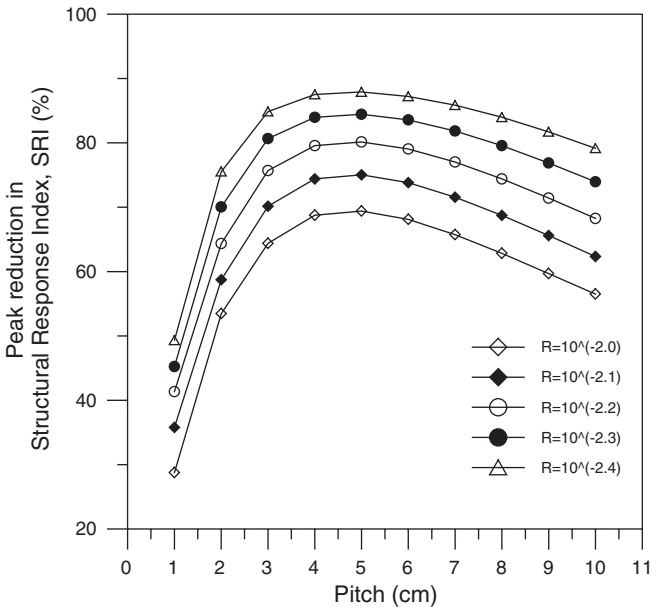

Figure 7. Efficiency curves of structural response index.

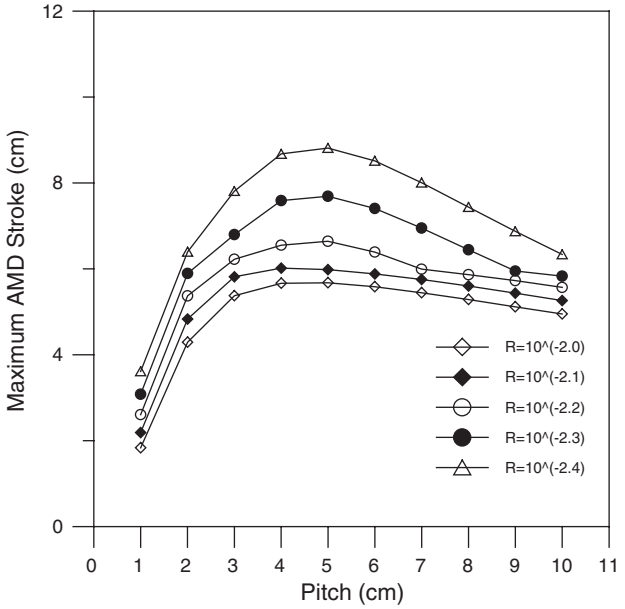

Figure 8. Effects of the pitch on AMD stroke.

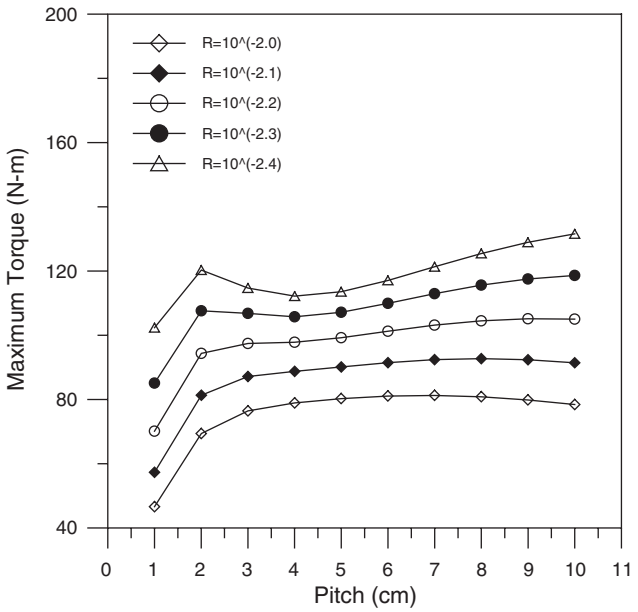

Figure 9. Effects of the pitch on torque.

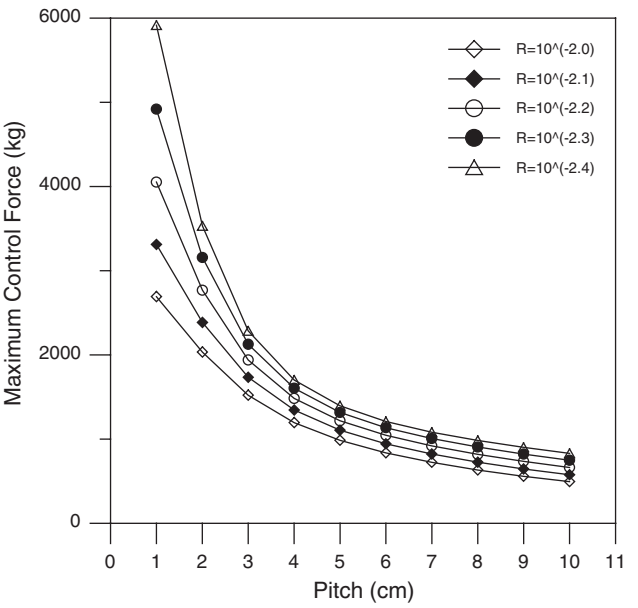

Figure 10. Effects of the pitch on control force demand.

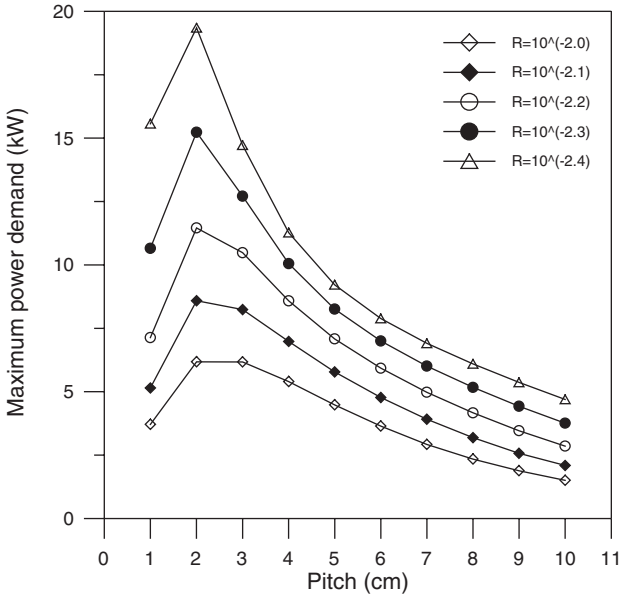

Figure 11. Effects of the pitch on power demand.

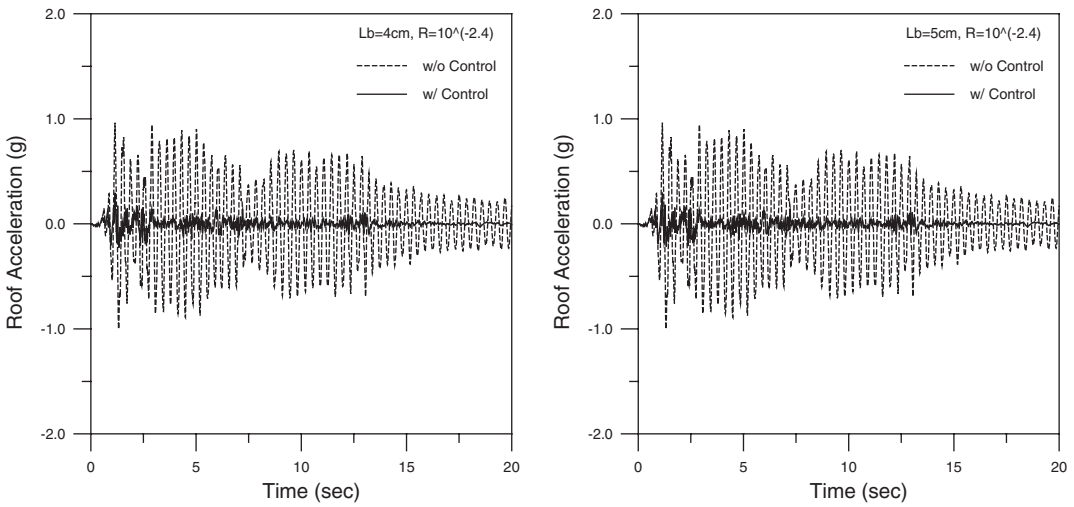

Figure 12. Comparison of roof acceleration responses ($R = 10^{-2.4}$).

the inertia term, $(2\pi/l_b)^2$, included in the mass matrix for smaller pitch sizes ($l_b = 1$ cm and $l_b = 2$ cm) is somewhat large, it demands more control forces to suppress the structural vibration. Figure 11 illustrates the maximum power demand of the servomotor. The power is calculated as $P = \max |u_T(\frac{2\pi}{l_b}\dot{\bar{x}}_a)|$. Again, the maximum power demand increases as R decreases and it tends to decrease with the pitch size, regardless of R.

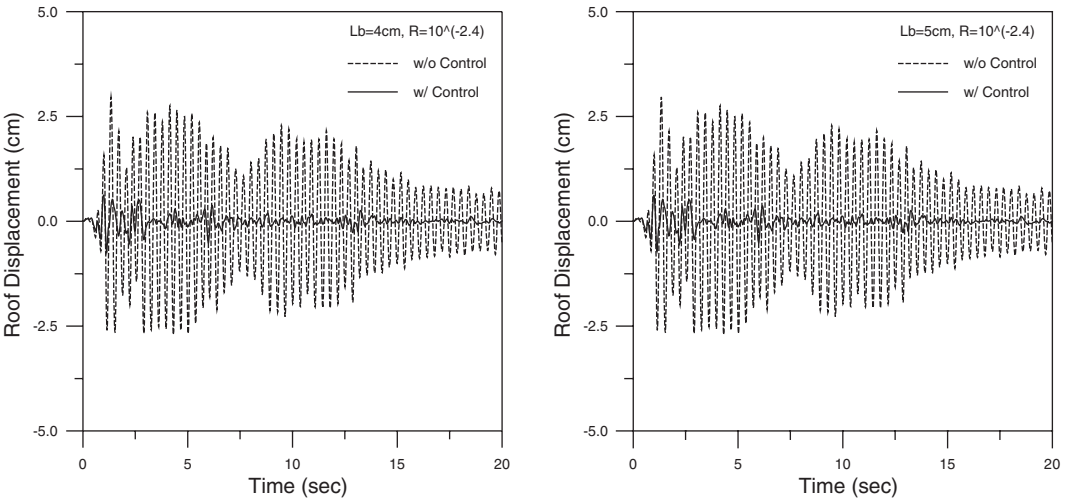

Figure 13. Comparison of roof displacement responses ($R = 10^{-2.4}$).

The roof acceleration history and the roof displacement history for the case of $R = 10^{-2.4}$ with $l_b = 4$ cm and $l_b = 5$ cm are also illustrated, respectively, in Figures 12 and 13, where large reductions of 71% (for $l_b = 4$ cm) and 70% (for $l_b = 5$ cm) in roof acceleration, and 75% ($l_b = 4$ cm) and 76% (for $l_b = 5$ cm) in roof displacement have been achieved. If the pitch size of the ball screw is appropriately adjusted, the control effectiveness of the AMD system can be greatly enhanced.

6. CONCLUSIONS

This study investigated an electrical active mass driver system for seismic structural control. The effects of the pitch size of the ball screw on the system performance were explored. Moreover, an instantaneous optimal direct output feedback control law was also derived alongside the hardware development. The feasibility of the proposed system was verified through numerical simulations of a five-story model structure under the conditions of the 1940 El Centro earthquake. In accordance with the simulation results, the conclusions are summarized as:

1. The desired stroke amplification of the mass block and the power demand of the servomotor could be adjusted via the ball screw pitch, which in turn affected the effectiveness and efficiency of the system.
2. The AMD system proved to be very effective within a certain range of the pitch (between $l_b = 4$ cm and $l_b = 5$ cm in this numerical example) while demanding less control force and power. The reductions of the peak responses of the model structure could reach as high as 70% if properly designed.
3. Despite the fact that only the velocity of the roof was measured as the feedback state, no spillover was observed by using the proposed direct output feedback control law. It was recommended as being favorable for practical implementation.

ACKNOWLEDGEMENTS

The authors would like to thank Dr L. L. Chung of the National Center for Research on Earthquake Engineering, Taiwan, R.O.C., for his valuable discussions. The authors are also grateful to the National Science Council of Taiwan, R.O.C. for the financial support of this research under grant no. NSC 90-2625-Z-009-003.

REFERENCES

1. Soong TT. State-of-the-art-review: Active structural control on civil engineering. *Engineering Structures* 1988; **10**:74–84.
2. Soong TT, Masri SF, Housner GW. An overview of active structural control under seismic loads. *Earthquake Spectra* 1991; **7**:483–505.
3. Housner GW *et al.* Special Issue, Structural control: Past, present, and future. *Journal of Engineering Mechanics* (ASCE) 1997; **123**(9):1–15.
4. Soong TT, Spencer BF, Jr. Supplemental energy dissipation: state-of-the-art and state-of-the-practice. *Engineering Structures* 2002; **24**:243–259.
5. Kobori T. Future direction on research and development of seismic-response-controlled structure. *Proceedings of the First World Conference on Structural Control* 1994, pp 19–31.
6. Reinhorn AM, Soong TT, Lin RC, Riley MA, Wang YP, Aizawa S, Higashino M. Active bracing system: a full-scale implementation of active control. Technical Report, NCEER-92-0020, NCEER/SUNY/Buffalo, 1992.
7. Reinhorn AM, Soong TT, Lin RC, Wang YP, Fukao Y, Abe H, Nakai M. 1:4 Scaled model studies of active tendon systems and active mass dampers for aseismic protection. Technical Report, NCEER-89-0026, NCEER/SUNY/Buffalo, 1989.
8. Soong TT. *Active Structural Control*: *Theory and Practice.* Wiley: New York, 1990.
9. Soong TT, Dargush GF. *Passive Energy Dissipation Systems in Structural Engineering.* Wiley: New York, 1997.
10. Aizawa S, Yamaguchi I, Kinoshila K, Yamaguchi N, Hayamizu Y, Fukao Y, Minewaki S, Abe H, Haniuda N. An experimental study on active mass damper—Part 2. Experiments of four-story model. (In Japanese), *Annual Meeting of Architectural Institute of Japan*, pp 899–904, 1987.
11. Fukao Y, Abe H, Kinoshila K, Haniuda N. An experimental research on active mass damper—Part 2. Comparison with test results and simulations. (In Japanese), *Annual Meeting of Architectural Institute of Japan*, pp 2254–2255, 1989.
12. Spencer BF, Jr, Dyke SJ, Deoskar HS. Benchmark problems in structural control: Part 1—Active mass driver system. *Earthquake Engineering and Structural Dynamics* 1998; **27**:1127–1139.
13. Chapman SJ. *Original*: *Electric Machinery Fundamentals*, 3rd edition. McGraw-Hill: New York, 1999.
14. Dote Y. *Servo Motor and Motion Control Using Digital Signal Processors.* Prentice-Hall: Englewood Cliffs, NJ, 1990.
15. Yamamura S. *AC Motors for High-Performance Applications*: *Analysis and Control.* Marcel Dekker: New York, 1986.
16. Hanselman DC. *Brushless Permanent-Magnet Motor Design.* McGraw-Hill: New York, 1994.
17. Fujinami T, Saito Y, Morishita M, Koike Y, Tanida K. A hybrid mass damper system controlled by H^{∞} control theory for reducing bending–torsion vibration of an actual building. *Earthquake Engineering and Structural Dynamics* 2001; **30**:1639–1653.
18. Saito T, Shiba K, Tamura K. Vibration control characteristics of a hybrid mass damper system installed in tall buildings. *Earthquake Engineering and Structural Dynamics* 2001; **30**:1677–1696.
19. Nakamura Y, Tanaka K, Nakayama M, Fujita T. Hybrid mass dampers using two types of electric servomotors: AC servomotors and linear-induction servomotors. *Earthquake Engineering and Structural Dynamics* 2001; **30**:1719–1743.
20. Kobori T. *Proceedings of the Second World Conference on Structural Control*, Kyoto, Japan, Vol. 1, 1998.
21. Robert L, Mott PE. *Machine Elements in Mechanical Design.* Second edition, Macmillan: New York, 1992.
22. Black PH, Adams OE. *Machine Design.* Third edition, McGraw-Hill: Singapore, 1981.
23. Wang Y-P, Lee C-L, Chen K-M. Seismic structural control using a novel high-performance active mass driver system. *Earthquake Engineering and Structural Dynamics* 2000; **29**:1629–1646.

